A New Magnetic-Field-Modulated Brushless Double-Rotor Machine

Jingang Bai[2], Ping Zheng[1,2], Luming Cheng[2], Shukuan Zhang[2], Jiaqi Liu[2], and Zhaoyue Liu[3]

[1]State Key Laboratory of Robotics and System, Harbin Institute of Technology, Harbin 150080, China
[2]Department of Electrical Engineering, Harbin Institute of Technology, Harbin 150080, China
[3]College of Engineering, Nanjing Agricultural University, Nanjing 210031, China

In this paper, a new magnetic-field-modulated brushless double-rotor machine (MFM-BDRM) is proposed, solving the contradictory problem of the electromagnetic performance and the mechanical strength of an MFM rotor in the traditional MFM-BDRMs. The operating principle of the proposed MFM-BDRM, including the speed and torque relations of the stator, the MFM rotor, and the permanent magnet (PM) rotor, is investigated by an analytical method. The magnetic field distribution law in the air gap, the back electromotive force, and the torque performance of the proposed MFM-BDRM are investigated. To obtain the maximum torque density, the influence of some key parameters, such as PM pole-arc coefficient, span ratio, and thickness of magnetic units, on the maximum torque is investigated. Besides, due to the rich magnetic-field harmonics with high rotating speed in the air gap, the distribution law of iron loss in the proposed MFM-BDRM is investigated. The PM-split method along the circumferential direction is employed to reduce the PM loss. Finally, the overall performance of this new MFM-BDRM is evaluated, including loss, efficiency, power density, and so on.

***Index Terms*— Brushless double-rotor machine (DRM), core loss, electromagnetic performance, hybrid electric vehicle (HEV), magnetic-field modulated (MFM), permanent magnet (PM) loss.**

I. Introduction

With the advantage of independent speed control of two rotors, the double-rotor machine (DRM) can be a promising candidate for the electrical continuously variable transmission in hybrid electric vehicles (HEVs) [1]–[3]. Since the DRM with brushes and slip rings has problems of extra losses, low reliability, and maintenance, the brushless DRM would be a preferable selection. The magnetic-field-modulated brushless DRM (MFM-BDRM), which is composed of the stator, the MFM rotor, and the permanent magnet (PM) rotor, is a typical brushless DRM [4], [5]. However, the analysis of the MFM-BDRM showed that the MFM rotor had a contradictory problem of electromagnetic performance and mechanical strength, due to the alternative placement of magnetic and nonmagnetic blocks [6].

In this paper, a new MFM-BDRM is proposed, solving the problem of the weak mechanical strength of MFM rotor in the traditional MFM-BDRMs and keeping the electromagnetic performance. As a new MFM-BDRM, the operating principle, the magnetic field distribution, the back electromotive force (EMF), and the torque performance are investigated. To obtain the maximum torque density, the design principle of some key parameters is investigated. Besides, to reduce the PM loss, the method of dividing the PM into several pieces along the circumferential direction is investigated. Finally, the overall performance of this new MFM-BDRM is evaluated, including loss, efficiency, power density, and so on.

II. Structure and Operating Principle

A. Structure

Traditional MFM-BDRM is composed of the stator, the MFM rotor, and the PM rotor, as shown in Fig. 1(a).

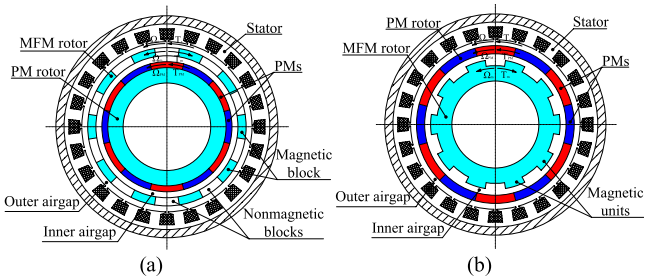

Fig. 1. Structures of MFM-BDRMs. (a) Traditional. (b) Proposed.

Its MFM rotor, which is formed by the alternative placement of magnetic and nonmagnetic blocks, is set in the middle of the stator and PM rotor. Therefore, this MFM rotor of the traditional MFM-BDRM has such a contradictory problem of the electromagnetic performance and the mechanical strength. On the one hand, due to rich harmonic waves in the air gap, the silicon steel sheet material is a preferable selection for the magnetic blocks to reduce harmonic losses. But the lamination of silicon steel sheet is difficult to obtain the satisfactory mechanical strength of the MFM rotor. On the other hand, to improve the mechanical strength of the MFM rotor, a whole solid iron can be selected as the magnetic block, but it can also produce a large eddy current loss and seriously reduce the motor performance. Hence, a new MFM-BDRM is proposed in this paper, as shown in Fig. 1(b). The proposed MFM-BDRM is also composed of the stator, the MFM rotor, and the PM rotor. Compared with the traditional MFM-BDRM, the main difference is that the MFM rotor of the proposed MFM-BDRM is set in the innermost layer and all magnetic units of the MFM rotor connect together. In this case, employing the lamination of silicon steel sheet can reduce harmonic losses as well as improve the mechanical integrity and further constitute a strong MFM rotor. Although the PM outer rotor is also faced with the manufacturing problem, the solid-construction PM will make the proposed MFM-BDRM much easier to be manufactured than the traditional one.

Manuscript received March 20, 2015; revised June 8, 2015; accepted June 14, 2015. Date of publication June 16, 2015; date of current version October 22, 2015. Corresponding author: P. Zheng (e-mail: zhengping@hit.edu.cn).

Color versions of one or more of the figures in this paper are available online at http://ieeexplore.ieee.org.

Digital Object Identifier 10.1109/TMAG.2015.2445917

TABLE I
PARAMETERS OF THE PROPOSED MFM-BDRM

Parameters	Value
Pole-pair number of the PM rotor	17
Pole-pair number of the stator	4
Number of magnetic units	21
Outer diameter of the stator	216 mm
Axial length of the MFM-BDRM	70 mm
Radial length of the outer air gap	1 mm
Radial length of the inner air gap	1 mm
Thickness of PMs	4 mm
Br (N35SH)	1.2T
Stator slots	24

B. Operating Principle

The proposed MFM-BDRM is working on the basis of the magnetic field modulation principle. In fact, the magnetic field modulation principle has been applied in magnetic gears, vernier machines, and magnetic-geared machines [7]–[9]. According to the analysis of magnetic field modulation principle [5]–[7], we can get

$$q = p + n \tag{1}$$

$$\Omega_s = \frac{n\Omega_{\mathrm{PM}}}{n-q} + \frac{-q\Omega_m}{n-q} \tag{2}$$

where p and n are the pole-pair number of stator and PM rotor, respectively; q is the number of magnetic units of the MFM rotor; Ω_s, Ω_{PM}, and Ω_m are the rotating speeds of the stator magnetic field, the PM rotor, and the MFM rotor, respectively.

From the view of a conservative lossless system [5], [6], we can get

$$T_m = -\frac{q}{p}T_s \tag{3}$$

$$T_{\mathrm{PM}} = \frac{n}{p}T_s \tag{4}$$

where T_s, T_m, and T_{PM} are the electromagnetic torques acting on the stator, the modulating ring rotor, and the PM rotor.

III. ELECTROMAGNETIC PERFORMANCE

Take the finite-element model with $p = 4$, $q = 21$, and $n = 17$ as an example to analyze the electromagnetic performance of the proposed MFM-BDRM. With magnetic property, working temperature, and cost in HEV application considered, the N35SH PM material is selected. In addition, the parameters are listed in Table I.

Since the magnetic field in the outer air gap can link with the stator windings, the flux density distribution and harmonic components in the outer air gap are calculated by finite-element method (FEM) at no load, as shown in Fig. 2, respectively. We can see that the largest harmonic component is the 17 pole-pair magnetic field, which is the same as the pole-pair number of the PM rotor. Besides, it is noted that a significant 4 pole-pair magnetic field, which has the same pole-pair number as the stator magnetic field, is obtained with the influence of the MFM rotor. The significant 4 pole-pair magnetic field will induce the back EMF in the stator windings and further produce the electromagnetic torque with the stator windings fed with the current.

The no-load back EMF $E_{\phi v}$ induced by each harmonic magnetic field can be calculated by

$$E_{\phi v} = 4.44 f_v K_{wv} N \Phi_v \tag{5}$$

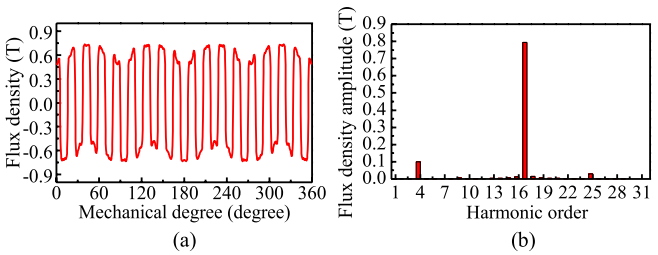

Fig. 2. Flux density distribution and harmonic components in the outer air gap. (a) Magnetic field waveform. (b) Harmonic analysis.

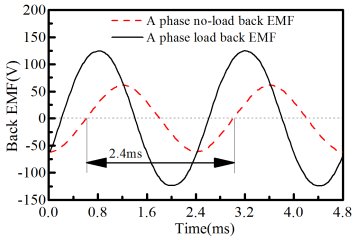

Fig. 3. No-load and load back EMF.

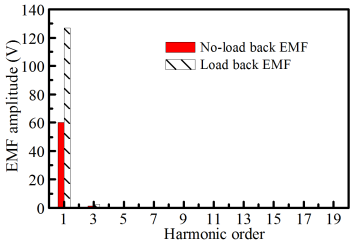

Fig. 4. Spectrum analysis of the no-load and load back EMF.

where f_v is the frequency of the vth harmonic magnetic field, K_{wv} is the winding factor of the vth harmonic magnetic field, N is the number of series turns per phase, and Φ_v is the vth harmonic flux per pole. The calculated no-load back EMF waveform of the stator windings by FEM and the corresponding spectral analysis are shown in Figs. 3 and 4. In the process of simulation, to meet the practical needs of HEVs, the speeds of the MFM rotor and the PM rotor are set to 2000 and 1000 r/min, respectively; in this case, the speed of magnetic field in the stator is 6250 r/min, based on (2). According to $60/\mathrm{p}\Omega_s$, the period of back EMF induced in windings per phase is 2.4 ms. From Figs. 3 and 4, we can see that the proposed MFM-BDRM has a highly sinusoidal back EMF, with the calculated distortion rates of no-load and load back EMF being 2.3% and 1.8%, respectively. This is mainly because that the stator windings adopt the integer-slot winding configuration based on the four pole pairs of the stator. Therefore, the winding factor of all harmonic fields with the noninteger times of 4 by calculation is zero. For the 17 pole-pair magnetic field ($K_{w17} = 0$), although its amplitude is the largest, it has no production of harmonic back EMF. Similarly, the load back EMF is also quite sinusoidal, because of the EMFs induced by harmonic components canceling out in windings per phase. It indicates that the proposed MFM-BDRM is more suitable for the sinusoidal current drive.

To show the torque performance of the proposed MFM-BDRM, the electromagnetic torque waveforms of the stator, the MFM rotor, and the PM rotor are calculated by FEM at rated load, as shown in Fig. 5. It can be seen that the torque ripples of the PM rotor and the MFM rotor are as

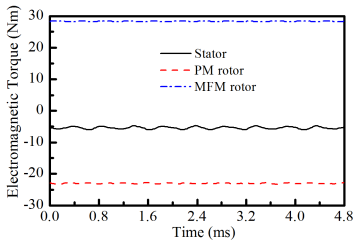

Fig. 5. Electromagnetic torque waveforms.

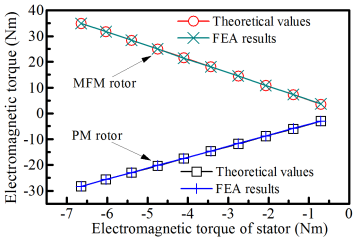

Fig. 6. Torque relation verification.

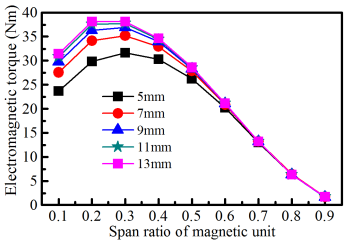

Fig. 7. Electromagnetic torque versus the span ratio of magnetic unit.

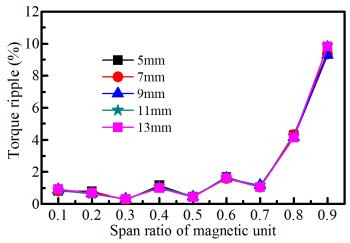

Fig. 8. Torque ripple versus the span ratio of magnetic unit.

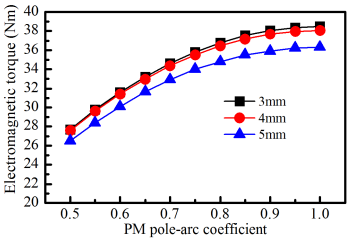

Fig. 9. Electromagnetic torque versus the PM pole-arc coefficient.

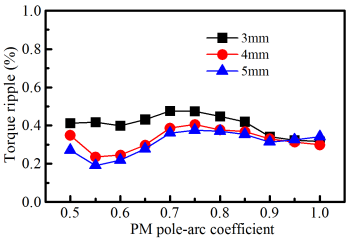

Fig. 10. Torque ripple versus the PM pole-arc coefficient.

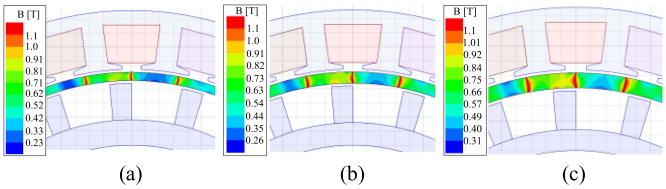

Fig. 11. Distribution of PM flux density at rated load for different PM-thickness topologies. (a) 3 mm. (b) 4 mm. (c) 5 mm.

low as 0.4% and 1.3%, respectively, which is an advantage of this machine. Fig. 6 shows the FEM results and theoretical values of the electromagnetic torque of both PM rotor and MFM rotor when the electromagnetic torque of stator changes. It is clear that the FEM results are in excellent agreement with theoretical values, proving the validity of the theoretical derivation of the torque transmitting characteristic.

IV. Analysis of the Torque Characteristic

The maximum output torque capability and the torque ripple are important performances for the MFM-BDRM. From the analysis of the torque performance above, we know that the electromagnetic torques of the stator, the MFM rotor, and the PM rotor are proportional. In the following text, the maximum output torque and torque ripple of the MFM rotor are taken as the research subject.

To obtain the maximum output torque, the influence of the span ratio and radial thickness of magnetic units is first investigated. It shows that the maximum torque of the MFM rotor can be obtained when the span ratio of magnetic unit is ~0.3 for any given radial thickness of magnetic unit, as shown in Fig. 7. Meanwhile, it shows that the torque ripple is the lowest at the optimal span ratio, as shown in Fig. 8. On the basis, the influence of the pole-arc coefficient and thickness of PM on the maximum torque of the MFM rotor is further investigated, as shown in Fig. 9. It shows that the maximum torque has a slight increase when the PM pole-arc coefficient is more than 0.9 for any given thickness of PM. The influence of the pole-arc coefficient and thickness of PM on the torque ripple is investigated, as shown in Fig. 10. It shows that the torque ripple is <0.5% when the PM parameters change. This indicates that the PM parameters have little effect on the torque ripple.

To ensure the PM working safely, the PM demagnetization problem is investigated. The safe value of PM flux density (N35SH) is not <0.25 T at 120 °C. The calculated demagnetization currents for different PM-thickness topologies in the short-circuit fault state are 19.5, 22, and 22.8 A, respectively. The corresponding flux density distribution in the PMs is shown in Fig. 11. The lowest values of PM flux density, with the PM thickness being 3, 4, and 5 mm, are 0.23, 0.26, and 0.31 T, respectively. Therefore, to ensure the PM working safely within 120 °C, the PM thickness should not be <4 mm for the proposed MFM-BDRM.

In HEV application, the MFM rotor is connected to the internal combustion engine (ICE), and the PM rotor is connected to the final gear and further to the wheels. A common HEV working condition is that the speed of ICE is keeping constant, and the speed of wheel is changing according to the requirement of the road condition. Meanwhile, during the speed-change process, the MFM-BDRM can transfer the ICE

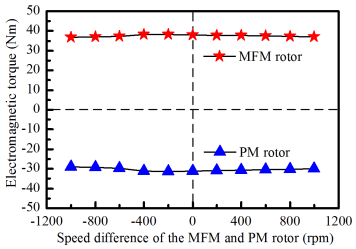

Fig. 12. Torque–speed characteristic of the proposed machine ($\Omega_m = 2000$ r/min).

TABLE II
IRON LOSS DISTRIBUTION OF DIFFERENT PARTS

Span ratio of magnetic units	No-load losses (W)			Load losses (W)		
	Magnetic units	Stator	PMs	Magnetic units	Stator	PMs
0.1	16.7	41.9	87.9	18.8	61.8	140.0
0.2	17.8	49.4	116.5	21.1	72.3	187.2
0.3	18.7	52.3	122.2	21.9	76.5	202.9
0.4	19.9	52.9	116.7	23.3	78.8	207.6
0.5	21.0	52.5	100.3	24.6	80.2	201.1
0.6	21.8	52.4	78.2	25.5	81.2	187.8
0.7	22.4	52.7	55.5	26.3	82.4	172.8
0.8	23.1	54.1	39.0	26.9	84.0	161.6
0.9	23.1	55.3	31.7	26.6	85.7	157.7

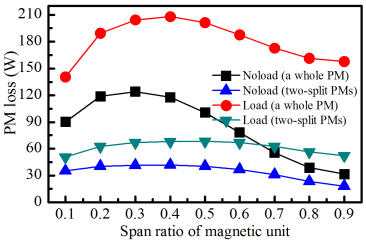

Fig. 13. Influence of circumferential PM-split method on PM loss.

torque to the final gear and further to the wheels. Therefore, the torque–speed characteristic of the proposed machine at rated load is shown in Fig. 12. It can be seen that the working region of the proposed machine is the rectangular one in HEV application.

V. ANALYSIS OF LOSS DISTRIBUTION

Due to the rich magnetic-field harmonics with high rotating speed in the air gap, the distribution law of iron loss in the proposed MFM-BDRM is investigated. Table II shows the distribution law of iron loss at no load and load with the change of the span ratio of magnetic units. It shows that the PM loss is ∼60% of the total iron loss at no load and load. Therefore, the PM-split method along the circumferential direction is employed to reduce the PM loss, which makes the PM loss reduced by ∼60%, as shown in Fig. 13. Finally, the performances of the proposed and the traditional MFM-BDRMs are listed in Table III. It can be seen that the proposed MFM-BDRM has advantages in torque ripple, but it also has disadvantages in efficiency and power density, compared with the traditional one.

VI. CONCLUSION

A new MFM-BDRM is proposed, solving the contradictory problem of the electromagnetic performance and the mechanical strength of MFM rotor in the traditional MFM-BDRM. The proposed one has advantages of highly sinusoidal back EMF and low torque ripple. The maximum torque can be obtained when the optimal span ratio is 0.3 for any given thickness of magnetic units. Meanwhile, the maximum torque has a slight increase when the PM pole-arc coefficient is more than 0.9. The distribution law of iron loss in the MFM-BDRM shows that the PM loss is ∼60% of the total iron loss. The PM-split method along the circumferential direction is employed to reduce the PM loss, which makes the PM loss reduced by ∼60%.

TABLE III
PERFORMANCES OF THE PROPOSED AND THE TRADITIONAL MFM-BDRMS

Performance parameter	Proposed MFM-BDRM	Traditional MFM-BDRM
Rated Power	5 kW	5kW
Torque of PM rotor	30 Nm	30 Nm
Torque ripple of PM rotor	0.4%	1.4%
Torque of MFM rotor	38Nm	38Nm
Torque ripple of MFM rotor	1.3%	1.7%
Power factor	0.61	0.61
Efficiency	91.4%	92.3%
Power density	0.55 kW/kg	0.76 kW/kg

ACKNOWLEDGMENT

This work was supported in part by the National Natural Science Foundation of China under Project 51325701, Project 51377030, and Project 51407042, and in part by Self-Planned Task (NO. 201504B) of State Key Laboratory of Robotics and System (HIT).

REFERENCES

[1] L. Mo, L. Quan, X. Zhu, Y. Chen, H. Qiu, and K. T. Chau, "Comparison and analysis of flux-switching permanent-magnet double-rotor machine with 4QT used for HEV," *IEEE Trans. Magn.*, vol. 50, no. 11, Nov. 2014, Art. ID 8205804.

[2] S. Niu, S. L. Ho, and W. N. Fu, "A novel double-stator double-rotor brushless electrical continuously variable transmission system," *IEEE Trans. Magn.*, vol. 49, no. 7, pp. 3909–3912, Jul. 2013.

[3] P. Pišek, B. Štumberger, T. Marčič, and P. Virtič, "Design analysis and experimental validation of a double rotor synchronous PM machine used for HEV," *IEEE Trans. Magn.*, vol. 49, no. 1, pp. 152–155, Jan. 2013.

[4] C.-T. Liu, H.-Y. Chung, and C.-C. Hwang, "Design assessments of a magnetic-geared double-rotor permanent magnet generator," *IEEE Trans. Magn.*, vol. 50, no. 1, Jan. 2014, Art. ID 4001004.

[5] J. Bai, P. Zheng, C. Tong, Z. Song, and Q. Zhao, "Characteristic analysis and verification of the magnetic-field-modulated brushless double-rotor machine," *IEEE Trans. Ind. Electron.*, vol. 62, no. 7, pp. 4023–4033, Jul. 2015.

[6] P. Zheng, J. Bai, C. Tong, Y. Sui, Z. Song, and Q. Zhao, "Investigation of a novel radial magnetic-field-modulated brushless double-rotor machine used for HEVs," *IEEE Trans. Magn.*, vol. 49, no. 3, pp. 1231–1241, Mar. 2013.

[7] H. Rashidi and D. Pishdad, "Integrated multispeed magnetic gears: A novel approach to design of magnetic transmission systems," *IEEE Trans. Magn.*, vol. 51, no. 4, Apr. 2015, Art. ID 8700308.

[8] G. Liu, J. Yang, W. Zhao, J. Ji, Q. Chen, and W. Gong, "Design and analysis of a new fault-tolerant permanent-magnet vernier machine for electric vehicles," *IEEE Trans. Magn.*, vol. 48, no. 11, pp. 4176–4179, Nov. 2012.

[9] C. Liu, K. T. Chau, and Z. Zhang, "Novel design of double-stator single-rotor magnetic-geared machines," *IEEE Trans. Magn.*, vol. 48, no. 11, pp. 4180–4183, Nov. 2012.